Theoretical Design of Topological Heteronanotubes - Supporting Information

Chen Hu,*,† Vincent Michaud-Rioux,† Wang Yao,‡ and Hong Guo†

E-mail: huchen@physics.mcgill.ca

In this Supporting Information, we provide supporting details of the calculation and further results of topological heteronanotubes(THTs). We organize into the following sections:

1. Electronic structure calculation and inter-wall distance optimization;
2. Chern number analysis;
3. Small-diameter THT;
4. Multi-period THT;
5. Reverse-ordered THT;
6. Commensurate double-wall heteronanotubes;
7. Zigzag-type THT and chiral-type THT;
8. Topological properties of double-wall CNT.

Section 1: Structure calculation and inter-wall distance optimization

In this work, electronic structures and topological properties are calculated using the real-space Kohn-Sham density functional theory (KS-DFT) as implemented in the RESCU package.[1] In our

*To whom correspondence should be addressed

†Center for the Physics of Materials and Department of Physics, McGill University, Montreal, Quebec H3A 2T8, Canada

‡Department of Physics and Center of Theoretical and Computational Physics, University of Hong Kong, Hong Kong, China

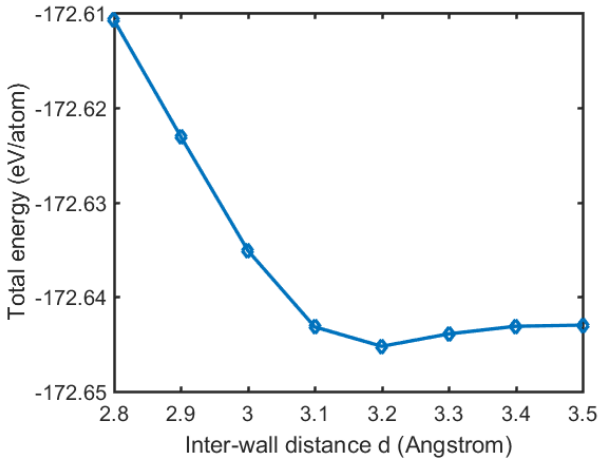

Figure S1: Dependence of total energy on the inter-wall distance in CNT(n,n)@BNNT(n+m,n+m) when $n = 96$ and $m = 1$.

calculations, single-zeta polarized (SZP) atomic orbital basis set and optimized norm conserving Vanderbilt (ONCV) pseudopotentials[2] were employed. The exchange-correlation was treated at the generalized gradient approximation level (GGA-PBE).[3] The real-space resolution was set to 0.3 Bohr and we adopted $15 \times 1 \times 1$ Monkhorst-Pack k-point sampling. For calculating the Chern number (topological charge) by integrating the Berry curvature flux, we adopted a fine 666×400 k-mesh in the Brillouin zone.

As for the armchair THT, the general form is CNT(n,n)@BNNT(n+m,n+m). Fig.1 in the main text shows the case of $n = 96$ and $m = 1$. We carefully optimized the inter-wall distance d by DFT relaxation. As shown in Fig.S1, the equilibrium distance d is found to be 3.2 Å where the total energy reaches minimum. While different n and m values - corresponding to different diameters of the CNT and BNNT, may take slightly different equilibrium inter-wall distance, we use d = 3.2 Å for all systems for simplicity and for comparing the main moiré related physics. Complicated geometrical investigation of double-wall moiré nanotubes is another interesting topic which calls for further studies.

It is noted that a spiral THT has an extremely large supercell. For example, the supercell of the CNT(16, 16)@BNNT(17, 17) THT in Fig.3 of the main text, shown by the orange rectangle in

Fig.4(a) of the main text, contains 8448 atoms. Such a large system presents a serious computational challenge which is met by the RESCU method[1] that uses the Chebyshev filtering technique[4] and other advanced computational mathematics to drastically increase computational efficiency, making it possible for calculating such large moiré systems self-consistently by Kohn-Sham DFT. Our DFT calculation by RESCU package took 16.5 hours to converge it using 400 computational cores.

Section 2: Chern number analysis

The topological helical channels originate from the valley-dependent Chern number C_V varying over the moiré period on the circumference in the topological heteronanotubes, as shown in Fig.2(d,e) of the main text. The sign of the C_V depends on the local atomic registry between the CNT and BNNT walls. For THTs with very a large diameter, the curvature effect can be neglected and the atomic registry and electronic property of *local* atomic configurations on the 1D tube can be well described by the corresponding 2D structure when the tube is opened. Here we show the dependence between C_V and local atomic registry by the model of massive Dirac Hamiltonian of graphene:[5]

$$H = \frac{\sqrt{3}}{2} at(q_x \tau_z \sigma_x + q_y \sigma_y) + \frac{\Delta}{2}\sigma_z, \tag{S1}$$

where a is the lattice constant, t is the hopping parameter, q is the momentum measured from one valley point, Δ is the on-site staggered potential, τ and σ are the Pauli matrices acting in the valley space and sublattice space of graphene, respectively. Analytically, the Berry's curvature can be obtained from its definition:

$$\boldsymbol{\Omega}_n(\boldsymbol{k}) = \boldsymbol{\nabla}_{\boldsymbol{k}} \times i\langle u_{n\boldsymbol{k}} | \boldsymbol{\nabla}_{\boldsymbol{k}} | u_{n\boldsymbol{k}} \rangle, \tag{S2}$$

where $|u_{n\boldsymbol{k}}\rangle$ is the periodic part of the Bloch states of band index n. Berry's curvature of the conduction band of Hamiltonian Eq.(S1) can be analytically derived:[5]

$$\boldsymbol{\Omega}(q) = \tau_z \frac{3a^2\Delta t^2}{2(\Delta^2 + 3q^2a^2t^2)^{3/2}}. \tag{S3}$$

where τ_z is the valley index: +1 for K and -1 for K'. The valley-dependent Chern number C_V is obtained by:

$$C_V = \frac{1}{2\pi}\int d^2q\,\mathbf{\Omega}(q) = \frac{1}{2}\tau_z sgn(\Delta). \tag{S4}$$

For a certain valley - such as valley K, $C_V = \frac{1}{2}$ or $-\frac{1}{2}$ when Δ is positive or negative, respectively. In double-wall heteronanotubes, the *local* on-site staggered potential Δ of the CNT lattice is given by the inter-wall interaction with the BNNT. We use the corresponding 2D mapping of Fig.2(b) in the main text to explain how Δ varies along the moiré period. When carbon atoms face to boron atoms, nitrogen atoms or hollow sites, we name them as B-site, N-sites and h-sites respectively. In BN, B (N) atoms are positively (negatively) polarized due to a large difference in their electronegativity. The π orbital of carbon atoms has attractive and repulsive interactions with B cations and N anions respectively.[6,7] Therefore, electrons in CNT preferentially locate at B-sites and avoid N-sites to reduce electrostatic energy. This tendency results to the on-site energy ordering: $E_{N-site} > E_{h-site} > E_{B-site}$. The on-site staggered potential Δ, defined by the on-site energy difference between two carbon sublattice sites, will change its sign along the local atomic registry which varies in a moiré period. This can be inferred by configurations in the green circles in Fig.2(b) of the main text. We conclude that the topological phase transition - the change of sign of C_V, is a result of the variation of atomic registry between the CNT and BNNT walls.

The valley-dependent Chern number is by integrating the Berry curvature Ω around particular valley point of the k-space, as shown in Eq.(S4). The calculation of the Berry curvature usually has two equivalent formulas: Eq.(2) in the main text and Eq.(S2) in this *Supporting Information*. The equivalence of these two can be proved by the perturbation theory and Kubo formula.[8,9] Eq.(S2) is a much simpler form and usually used to calculate the Berry curvature analytically. The other formula, Eq.(2) in the main text is usually used in the numerical calculation of the Berry curvature to avoid gauge problem (random phase of numerical wavefunctions).[8] In this method, the velocity operators v_x and v_y are exploited, the elements of which are defined as:

$$\langle \psi_{q\boldsymbol{k}} | v_\alpha | \psi_{p\boldsymbol{k}} \rangle = \left\langle u_{q\boldsymbol{k}} | \frac{\partial H(\boldsymbol{k})}{\partial k_\alpha} | u_{p\boldsymbol{k}} \right\rangle, \tag{S5}$$

where α can be taken as x or y, $H(\boldsymbol{k}) = e^{-i\boldsymbol{k}\cdot\boldsymbol{r}} H e^{i\boldsymbol{k}\cdot\boldsymbol{r}}$, $|u_{\boldsymbol{k}}\rangle$ is the periodic part of the Bloch states and other notations are the same as in the main text.

Section 3: Small-diameter THT

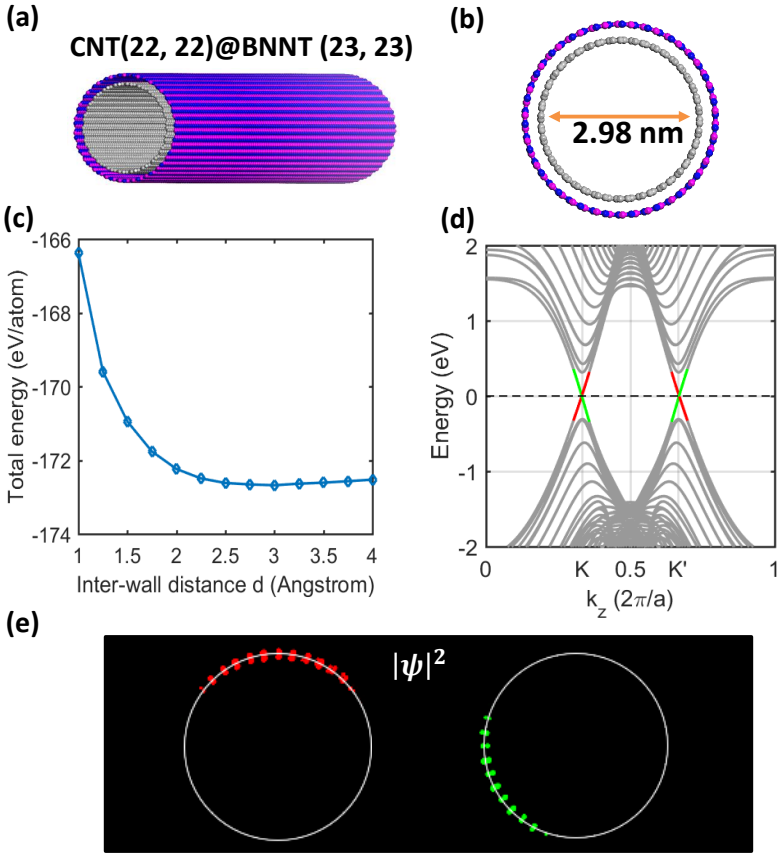

Figure S2: (a) Geometric structure of CNT(22,22)@BNNT(23,23), with the inner diameter of 2.98 nm as shown in the cross-section view of (b). (c) Dependence of total energy on the inter-wall distance. (d)Band structure of this THT. Gray lines are bulk bands and red (green) lines are helical channels - same as those of Fig.1 in the main text. (e) Spatial distribution of modular squared wave functions $|\psi|^2$ along the circumference of the topological helical channels in (d). The plotted isosurfaces are 7×10^{-8} a.u.

The general form of armchair THT is CNT(n,n)@BNNT(n+m,n+m). In the Fig.1 of the main text, to be specific but without losing generality, we study a particular case of n = 96 as an example to demonstrate the topological physics and phenomenon in THTs. In the experiment, the small-diameter CNTs, typically with the diameter below 4-5 nm, are most common and easily fabricated due to their stable circular geometric structures.[10,11] As a result, in this section we investigate a small-diameter case: CNT(22,22)@BNNT(23,23), with the diameter of 2.98 nm as shown in Fig.S2(b). Structural relaxation of Fig.S2(c) shows that the optimized inter-wall distance is around 3 Å. In Fig.S2(d) and (e), it is shown that the topological helical channels still appear in the band structure and their wavefunctions are located at two different regions (topological conducting pathways), similarly as the large-diameter THT in Fig.1 of main text. In the small-diameter THT, the geometric curvature effect is much larger than that in the large-diameter case. Our result reveals that the scheme of THT is general to a broad range of tube diameters, as well as structural robustness against the curvature effect in small-diameter tubes. We note that in previous study the similar property of topological structural robustness has also been found in 2D free-standing wavelike moiré patterns where the moiré -induced topological valleytronics can be against huge structural corrugations.[12]

Section 4: Multi-period THT

The general form of armchair THT is CNT(n,n)@BNNT(n+m,n+m), where various nanotube indexes (m and n) can provide essentially infinite possibilities for the type of THTs. When m = 1 as discussed in the Fig.1-2 of the main text, one moiré period locates along one circumference, which we shall name as 1-THT (single-period THT). In Fig.S3, we investigate several multi-period THTs with m = 2, 3, 4. Shown in the 2D mappings of Fig.S3(a-c), the value of m equals the number of moiré periods along one circumference, and each moiré period is n/m unit-cell length which includes two topological phase transition points (two topological moiré edges). Thus, the number of helical states is also determined by m. The calculated band structures in Fig.S3(d-f) show that besides the linear helical channels, there are also gapped ones arising inside the bulk band gap,

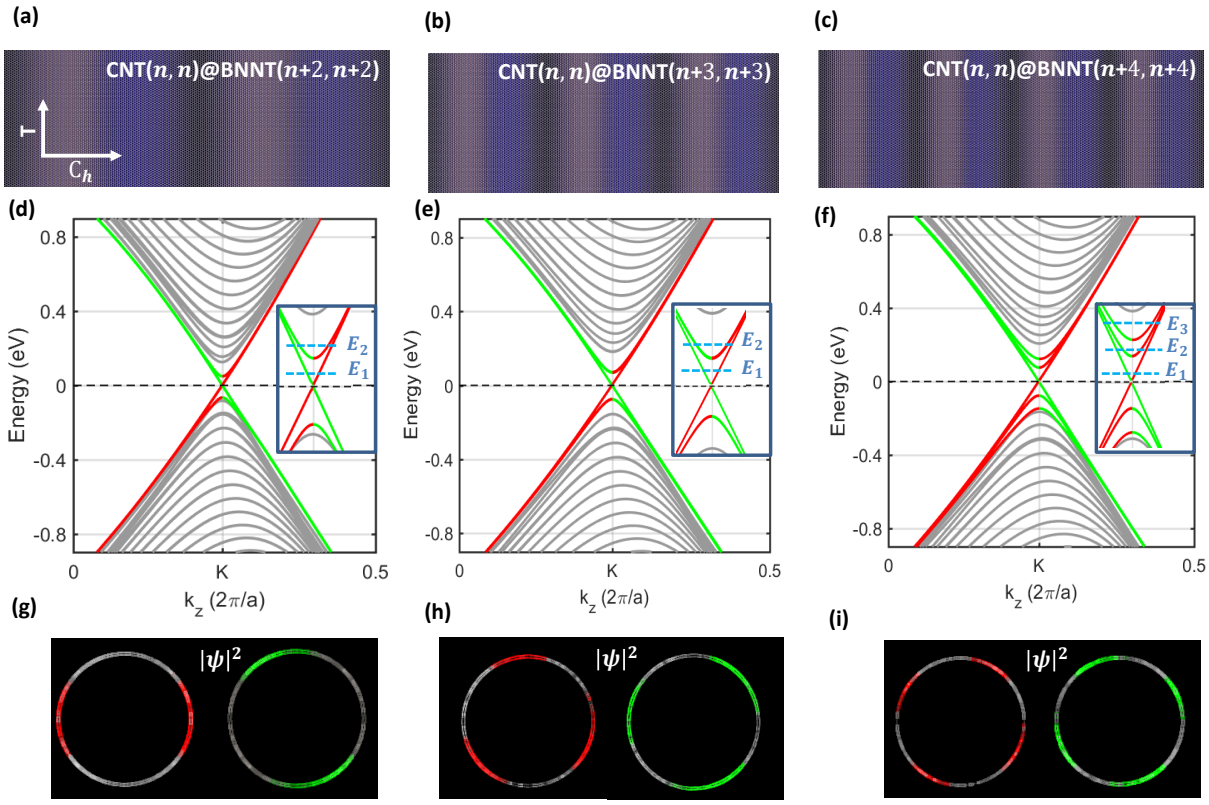

Figure S3: (a-c) 2D mapping of THTs with different values of m. n = 96 for all cases. (d-e) Band structures of the corresponding THT where insets focus on the topological bands near the Fermi level. Gray lines are bulk bands and red (green) lines are helical channels similar to those in Fig.1. E_1, E_2 and E_3 are different chemical potentials. (g-i) Spatial distribution of modular squared wave functions $|\psi|^2$ along the circumference of the topological helical channels in (d), (e) and (f), respectively. The plotted isosurfaces are 2.2×10^{-9} a.u.

and the total number of helical channels equals m (note that in Fig.S3(e,f) the group of helical states nearest to the Fermi level is two-fold degenerate). The wave functions in Fig.S3(g-i) show the circular distributions and numbers of the the conducting pathways (topological moiré edges) in the THTs. This result suggest that the modulation of chemical potential can provide a practical way to tune the quantized conductance of the multi-period THTs: for 2-THT ($m = 2$) in Fig.S3(d), $G = 2G_0, 4G_0$ when $\mu = E_1, E_2$; for 3-THT in Fig.S2(e), $G = 2G_0, 6G_0$ when $\mu = E_1, E_2$; and for 4-THT in Fig.S2(f), $G = 2G_0, 6G_0, 8G_0$ when $\mu = E_1, E_2, E_3$.

Section 5: Reverse-ordered THT

In the main text we focus on the THT formed by inner CNT and outer BNNT. On the experimental side, another system with a reversed order, outer CNT and inner BNNT, is also feasible.[13] In this case, m is usually negative of the general form CNT(n,n)@BNNT(n+m,n+m). In such systems, the key condition of the moiré topological physics, i.e. the moiré atomic registries varying along the circumference, still exists. As a result, the helical channels arise as shown in Fig.S4.

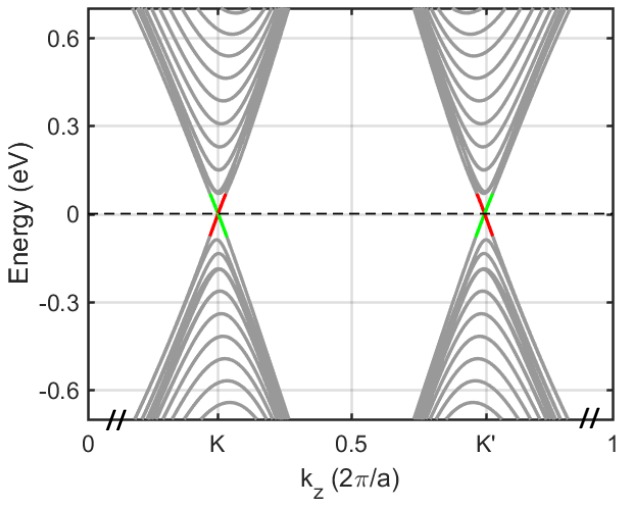

Figure S4: Band structure of the reverse-ordered THT: CNT(n, n)@BNNT(n+m,n+m) with $n = 96$ and $m = -1$. Gray lines are bulk bands and red (green) lines are helical channels - same as those of Fig.1 in the main text.

Section 6: Sublattice symmetry and commensurate double-wall heteronanotubes

The pristine metallic CNT is gapless, due to the sublattice symmetry (or spatial inversion symmetry) of the hexagonal lattice, as in the pristine graphene.[14] When an extra on-site staggered potential Δ is added, the sublattice symmetry is broken so that the two sublattices of CNT become located at different chemical environments, giving rise to a finite bulk band gap in CNT. In the CNT@BNNT heteronanotubes, BNNT wall can practically provide the on-site staggered potential, due to the large difference of electronegativity between boron and nitrogen atoms. A similar phenomenon was known in 2D systems.[7,12,15] Therefore, a bulk band gap opens in the CNT@BNNT heteronanotube systems, as shown in Fig.1(f) of the main text.

When $m = 0$ in the general form CNT(n,n)@BNNT(n+m,n+m), along the circumference the atomic registry is commensurate rather than a moiré structure. A bulk band gap still appears in the Dirac point as shown in Fig.S5, due to the sublattice symmetry breaking. However, no topological helical state appears since no moiré structure is formed in such a tube.

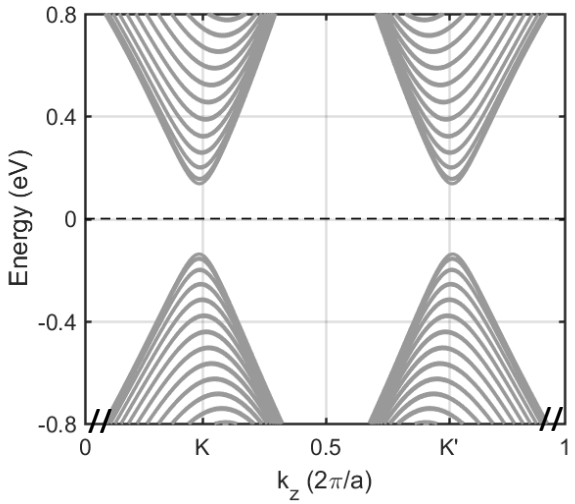

Figure S5: Band structure of the commensurate double-wall heteronanotubes: CNT(n, n)@BNNT(n+m,n+m) with $n = 96$ and $m = 0$.

Section 7: Zigzag-type THT and chiral-type THT

For zigzag-type THT, i.e. CNT(n, 0)@BNNT(n+m, 0), as shown in Fig.S6(a) no helical state appears inside the band gap. This is because indices K and K' are mixed together due to folding of the reciprocal space.[12,16] We conclude that zigzag heteronanotubes are not topological.

For chiral-type THT, the topological moiré edges are along the chiral direction. The topological helical states appear as shown in Fig.S6(b), similarly as the armchair-type THT in Fig.1 of the main text.

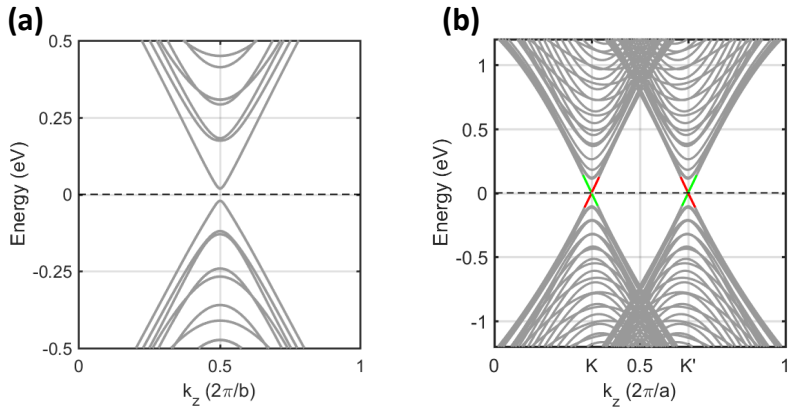

Figure S6: (a) Band structure of zigzag THT: CNT(n, 0)@BNNT(n+m, 0) with n=96 and m=1. b is the lattice constant of the transnational vector with a value of 4.26 Å. (b) Band structure of chiral THT: CNT(100, 25)@BNNT(104, 26) a is the lattice constant of the transnational vector with a value of 6.50 Å. Gray lines are bulk bands and red (green) lines are helical channels - same as those of Fig.1 in the main text.

Section 8: Topological properties of double-wall CNT

In the main text we focus on the most representative THT: CNT@BNNT. In fact, similar topological physics occurs in other tubular materials, here we investigate a double-wall CNT system where two *opposite* local stackings (AB and BA) locate on the circumference of the double-wall tube, according to the 2D mapping in Fig.S7(b). Due to its excellent mechanical strength and thermal/chemical stability, double-wall CNT is considered a promising material for nano-devices.[17]

With an electric field pointing along the radial direction, the AB and BA local stacking configurations obtain opposite staggered potentials: $\Delta_{AB} = -\Delta_{BA}$. According to Eq.(4) above, one obtains:

$$C_V(AB) = -C_V(BA). \tag{S6}$$

We therefore conclude that between these two local stacking configurations, the topological moiré edges emerge to support helical channels. All the topological properties in the THT of CNT@BNNT discussed in the main text can be established in double-wall CNT. The double-wall CNT is not a heteronanotube since both walls are carbon, therefore the topological moiré edges require a radial electric field to establish: such as field can be produced by a charged wire threading the CNT.

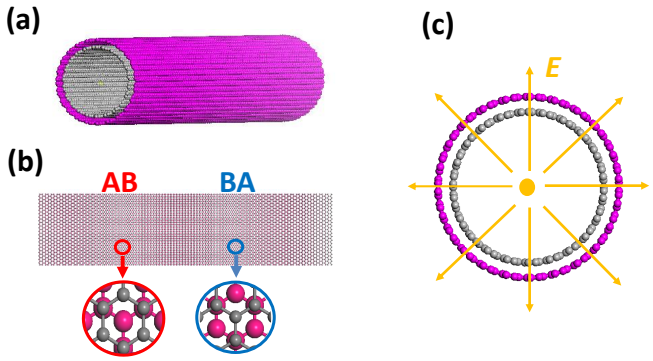

Figure S7: (a) Armchair double-wall CNT of CNT(n,n)@CNT(n+m,n+m). Here we take m=1 for example. The carbon atoms of outer CNT are plotted by purple balls to distinguish from those of the inner CNT wall (grey color). (b) The 2D mapping of (a). AB and BA are two local stackings. (c) A schematic plot of a radial electric field (orange arrows) that induces the topological states.

References

(1) Michaud-Rioux, V.; Zhang, L; Guo, H. J. Comput. Phys. **2016**, 307, 593.

(2) Hamann, D. R.; Phys. Rev. B **2013**, 88, 085117.

(3) Perdew, J. P. et al. Phys. Rev. B **1992**, 46, 6671.

(4) Zhou,Y; Saad, Y.; Tiago, M. L.; Chelikowsky, J. R. Phys. Rev. E **2006**, 74, 066704.

(5) Xiao, D.; Yao, W.; Niu, Q.; Phys. Rev. Lett. **2007**, 99, 236809.

(6) Fan, Y. et al. App. Phys. Lett. **2011**, 98, 083103.

(7) Hu, C.; Michaud-Rioux, V.; Kong, X.; Guo, H. Phys. Rev. Mater. **2017**, 1, 061003(R).

(8) Wang, X.; Yates, J. R.; Souza, I.; Vanderbilt, D. Phys. Rev. B **2006**, 74, 195118.

(9) Gradhand, M.; Fedorov, D. V.; Pientka, F.; Zahn, P.; Mertig, I.; Györffy, B. L. J. Phys. Condens. Matter. **2012**, 24, 213202.

(10) Zhang, C. et al. ACS Nano **2012**, 6, 6023.

(11) Motta, M. et al. Adv. Mater. **2007**, 19, 3721.

(12) Hu, C.; Michaud-Rioux, V.; Yao, W.; Guo, H. Phys. Rev. Lett. **2018**, 121, 186403.

(13) Nakanishi, J. R. et al. Sci. Rep. **2013**, 3, 1385.

(14) Charlier, J.; Blase, X.; Blase, S. Rev. Mod. Phys. **2007**, 79, 677.

(15) Giovannetti, G.; Khomyakov, P. A.; Brocks, G.; Kelly, P. J.; Van Den Brink, J.; Phys. Rev. B **2007**, 76, 073103.

(16) Abergel, D. J. Phys. Condens. Matter. **2017**, 29, 075303.

(17) Shen, C.; Brozena, A. H.; Wang, Y. Nanoscale **2011**, 3, 503.